LA-9912-MS

Los Alamos National Laboratory is operated by the University of California for the United States Department of Energy under contract W-7405-ENG-36.

Reaction-Path Calculations of Groundwater Chemistry Mineral Formation at Rainier Mesa, Nev

HYDROLOGY DOCUMENT NUMBER 261

Los Alamos Los Alamos National Labor
Los Alamos, New Mexico 8

This report was prepared by the Los Alamos National Laboratory as part of the Nevada Nuclear Waste Storage Investigations managed by the Nevada Operations Office of the US Department of Energy. Based upon their applicability to the investigations, some results from the Radionuclide Migration Project, managed by the Nevada Operations Office of the US Department of Energy, are included in this report.

Edited by Jody Heiken, INC Division

LA-9912-MS

UC-70
Issued: December 1983

Reaction-Path Calculations of Groundwater Chemistry and Mineral Formation at Rainier Mesa, Nevada

Jerry F. Kerrisk

Los Alamos National Laboratory
Los Alamos, New Mexico 87545

REACTION-PATH CALCULATIONS OF GROUNDWATER CHEMISTRY AND MINERAL FORMATION AT RAINIER MESA, NEVADA

By

Jerry F. Kerrisk

ABSTRACT

Reaction-path calculations of groundwater chemistry and mineral formation at Rainier Mesa, Nevada, have been done using a model of volcanic-glass dissolution by water that is initially saturated with CO_2. In the reaction-path calculation, rate processes control the availability of species through dissolution of volcanic glass, and equilibrium processes distribute the species between the aqueous phase and mineral phases in equilibrium at each step in the reaction path. The EQ3/6 chemical-equilibrium programs were used for the calculation. Formation constants were estimated for three zeolites (clinoptilolite, mordenite, and heulandite), so they could be considered as possible mineral precipitates. The first stage of mineral evolution, from volcanic glass to a cristobalite, smectite clay, and zeolite mixture, was modeled quite well. Predicted aqueous-phase compositions and precipitates agree with observations at Rainier Mesa and other Nevada Test Site areas. Further mineral evolution, to quartz, clay, analcime, and albite mixtures, was also modeled. Decreasing aqueous silica activity from the first stage, where cristobalite precipitates, to later stages, where quartz is present, was the controlling variable in the mineral evolution.

I. INTRODUCTION

Yucca Mountain, which is on and adjacent to the Nevada Test Site (NTS) in south-central Nevada, is being studied as a potential site for storage of high-level radioactive waste. These studies are part of the Nevada Nuclear Waste

Storage Investigations, which is managed by the Nevada Operations Office of the US Department of Energy. The mineralogy and water chemistry of a number of regions near Yucca Mountain have been studied in the past (Hoover 1968; Essington and Sharp 1968; White 1979; White et al. 1980; Moncure et al. 1981). The presence of zeolites and clays, with their excellent sorptive capabilities, is one of the justifications for considering this area for a waste repository (Waters and Carroll 1981; Caporuscio et al. 1982). Thus, the stability of these minerals under natural conditions and under the long-term perturbations anticipated from a repository is an important consideration for the site.

The reaction of groundwater with volcanic glass in the tuff near Yucca Mountain has been proposed as the primary mechanism for formation of the mineral assemblage that is currently observed (Hoover 1968). In one particular location, Rainier Mesa in the north-central section of NTS, studies of the groundwater chemistry, mineral assemblage, and volcanic-glass dissolution rates have led to proposal of a specific model for the area (White et al. 1980; Claassen and White 1978). In the model, water saturated with CO_2 reacts with volcanic glass. The various species composing the glass are leached or dissolved from the glass at different rates. Groundwater chemistry is related to the relative dissolution rates of species from the glass and the minerals that precipitate during the dissolution process. Claassen and White (1978) performed a material-balance calculation by using their measured dissolution rates and assuming precipitation of a montmorillonite clay with a specific composition to calculate the sodium, potassium, calcium, and magnesium composition of the groundwater and to compare it with observed compositions.

Mineralogy of this area has been studied at Rainier Mesa (White et al. 1980), Yucca Mountain (Waters and Carroll 1981; Caporuscio et al. 1982), Pahute Mesa (Moncure et al. 1981), and NTS in general (Hoover 1968). A sequence of stages in mineral evolution has been defined in these studies. The initial stage is the original volcanic glass. This is followed by a cristobalite, smectite clay, and zeolite (clinoptilolite and mordenite) mixture. Interstitial water compositions at Rainier Mesa are generally associated with progression from the initial volcanic glass to this stage (White et al. 1980; Claassen and White 1978). The next stage in mineral evolution is a quartz, analcime, and illite mixture, and the final product is a quartz, albite, and potassium-feldspar mixture, with calcite possibly present. These stages obviously represent an idealization of continuous changes that occur; however,

they are useful because there are large areas at NTS where minerals from the various stages predominate.

This paper describes reaction-path calculations of groundwater chemistry and mineral formation that are based on the model proposed by Claassen and White (1978). The reaction-path calculation models an essentially irreversible process (the dissolution of volcanic glass and precipitation of other minerals) as a sequence of partial equilibrium states (Helgeson 1968; Helgeson et al. 1969; Wolery 1979). The initial state of the system is water saturated with CO_2 at the temperature of interest. At each subsequent step in the sequence, additional glass dissolution products are added to the system in amounts proportional to their relative dissolution rates. An equilibrium calculation is performed to distribute the various species among the aqueous and mineral phases that are in equilibrium under the conditions of that step. The result of the calculation is a sequence of aqueous-phase compositions and mineral assemblages that would exist if the overall process were controlled by glass dissolution and all other processes were in equilibrium. The reaction-path calculation does not describe the overall irreversible process as a function of time, but in terms of a variable called the reaction progress. For these calculations, reaction progress is proportional to the amount of dissolution of volcanic glass. A direct relation between predicted system compositions and time cannot be made without additional rate data. Although actual dissolution rates were measured for the Rainier Mesa glass, the relation between time and the predicted compositions was not established here because it would have required an assumption about glass surface area available for dissolution (White et al. 1980; Claassen and White 1978).

The calculations presented here represent a very simplified model of a complex geologic system. Only the major chemical components are included in the model, and only equilibrium processes are considered at each step in the reaction path. However, the calculations do represent a step in the direction of a more quantitative treatment of the relation between groundwater and minerals at NTS. In this respect, they provide a test of whether equilibrium processes are important in controlling the mineral assemblage. The model also provides a tool for examining effects of changes in various parameters (temperature, for example) on equilibrium groundwater chemistry and mineral assemblages.

The EQ3/6 chemical equilibrium computer programs were used for these calculations (Wolery 1979; Wolery 1980). Although the EQ3/6 data base contains thermodynamic data for about 200 minerals, data for a number of the zeolites observed at Rainier Mesa have not been determined. Formation-constant data for clinoptilolite, heulandite, and mordenite were estimated and added to the data base for these calculations. Thus, the calculations represent a test of the consistency of the zeolite thermodynamic data as well as a test of the model.

Subsequent sections of this paper describe the (1) reaction-path calculation model, (2) zeolite thermodynamic data estimates, (3) calculated aqueous-phase compositions and mineral assemblages compared with observed data, and (4) implications of this work for Rainier Mesa and Yucca Mountain. Most of the comparisons are made with data from Rainier Mesa. However, because of the similarities between Rainier Mesa and Yucca Mountain, the models and results discussed here should also be applicable to Yucca Mountain. As more data become available from Yucca Mountain, more detailed comparisons will be made.

II. REACTION PATH MODEL

The reaction-path calculation described here represents an attempt to calculate groundwater composition (major components) and mineral formation (major minerals) at Rainier Mesa. The physical model describing the mineral-formation process is based on the proposal of Claassen and White (1978). Water saturated with CO_2 at pH 4.5 (2.26 mmolal in total carbonate at 25°C) from aerobic biological activity in the soil zone serves as the initial aqueous phase. This water reacts with volcanic glass; the glass dissolution process adds various species to the aqueous phase. The reaction-progress variable in the reaction-path calculation is a measure of the extent of glass dissolution. As dissolution proceeds, the aqueous phase becomes saturated with respect to various minerals. These minerals are allowed to precipitate, but it is assumed that they remain in contact with the aqueous phase. Thus, a mineral that precipitates early in the reaction path may redissolve later as conditions such as pH or cation concentrations change. This procedure is physically equivalent to a closed system in which static water saturates the tuff or in which water flow rates are so low that contact is maintained for long periods of time.

White et al. (1980) measured dissolution rates of $SiO_2(aq)$, Na^+, K^+, Ca^{2+}, and Mg^{2+} at 25°C from Rainier Mesa volcanic glass as a function of pH. Their results showed an initial rapid dissolution rate followed by a steady-state (parabolic) rate over longer times. Following the assumption of Claassen and White (1978), steady-state rates were used here. Because the reaction-progress variable is not directly related to time, only relative dissolution rates were needed for these calculations. The dissolution rates were normalized so that the $SiO_2(aq)$ dissolution rate was 1. Under these conditions, the reaction-progress variable is equal to the moles of $SiO_2(aq)$ dissolved from the glass. Dissolution rates for $SiO_2(aq)$ and K^+ were found to be essentially independent of pH, whereas rates for Na^+, Ca^{2+}, and Mg^{2+} decreased with increasing pH (White et al. 1980). Figure 1 shows a plot of the dissolution rates of these five species used for the calculations.

To precipitate most of the minerals observed at Rainier Mesa, it was necessary to also have aluminum and iron in the calculation. Dissolution rates for these species were not measured. It was assumed that the Al^{3+} dissolution rate [relative to $SiO_2(aq)$] was constant and was the same as the aluminum/silicon ratio of the Rainier Mesa volcanic glass (White et al. 1980). The rate used was 0.22 moles of Al^{3+} per mole of $SiO_2(aq)$. Iron was not determined in this glass; a constant dissolution rate for Fe^{3+} was assumed, based on compositions of similar volcanic glasses found near Rainier Mesa (Essington and Sharp 1968). The rate used was 0.02 moles of Fe^{3+} per mole of $SiO_2(aq)$. Ferric iron was assumed to be the dissolution product because the initial aqueous phase was taken as oxidizing, being in contact with $O_2(g)$ at 0.2 atm fugacity (Noble 1967). Figure 1 also shows the nominal dissolution rates of Al^{3+} and Fe^{3+} plotted with the other dissolution-rate data. Because Al^{3+} and Fe^{3+} dissolution rates were assumed rather than measured, some reaction-path calculations were done with higher and lower dissolution rates for these species to assess the effect of different rates on the results.

As proposed by Claassen and White (1978), the dissolution process is actually an ion-exchange reaction in which H^+ from the aqueous phase is exchanged for the cations from the volcanic glass to maintain electrical neutrality. This reaction was modeled by assuming that OH^- is one of the dissolution products and by calculating the OH^- dissolution rate to maintain electrical neutrality (see Fig. 1). The technique of adding aqueous species to the aqueous phase to simulate glass dissolution ignores the detailed

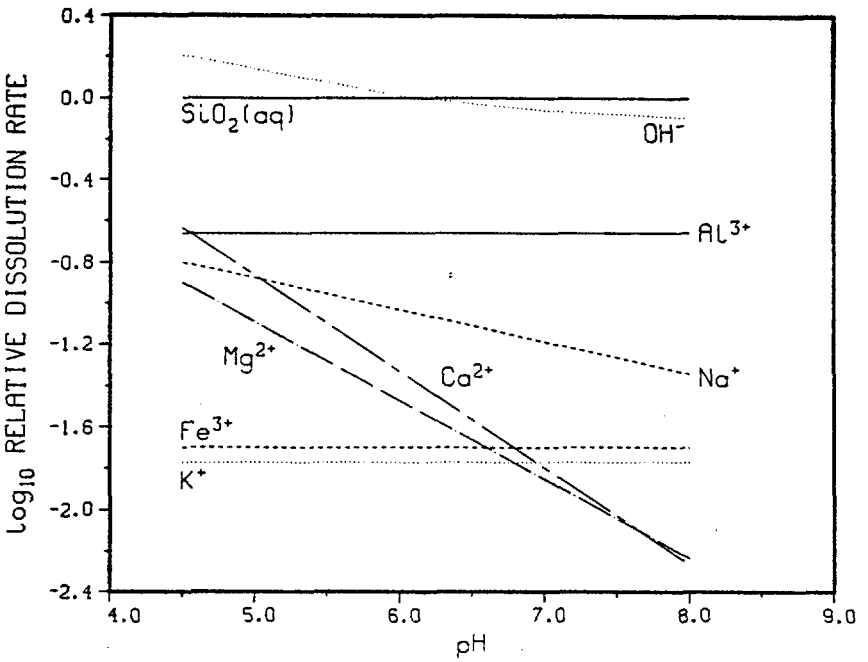

Fig. 1. Volcanic-glass dissolution rates.

mechanism of dissolution. However, the use of measured dissolution rates has accounted for observed behavior for most of the species in the glass. A better calculational model could undoubtedly be developed if mechanisms of glass hydration and dissolution were understood more quantitatively. At this stage of development, however, the dissolution model is probably adequate in comparison with other parts of the overall model.

For the calculations, no limit was placed on the quantity of any species available from the glass. This approach effectively assumes that the quantity of glass available for dissolution is large compared to the quantity of water and follows the same assumption made by Claassen and White (1978) in their calculation. Calculations were run to a particular value of the reaction progress (0.2 to 0.8), depending on the case being considered.

During the reaction-path calculation, if the aqueous phase becomes supersaturated with respect to a particular mineral, it is assumed that the mineral precipitates. The amount of the precipitate is calculated to just maintain saturation in the aqueous phase. In reality, many groundwaters are supersaturated with respect to a number of minerals. This is particularly true for silica minerals such as quartz and chalcedony. To simulate slow precipitation kinetics, precipitation of particular minerals can be suppressed; that is, the minerals can be removed from the data base for a calculation. This procedure

was followed with quartz and chalcedony for many of the calculations to increase the $SiO_2(aq)$ activity and with other minerals to change other aqueous-phase activities. Although the method of suppressing precipitation of particular minerals to simulate kinetic constraints on precipitation is a rough approximation to reality, it does serve to bracket the expected conditions of the system and thus can give useful information.

The reaction-path calculations were done with the EQ3/6 chemical-equilibrium computer programs, version 3175B, which were released in August 1982 (Wolery 1979; Wolery 1980). The EQ3 program, which performs a speciation calculation at the start of a run, was used without modification. The EQ6 program, which performs the reaction-path calculation, was modified to allow the dissolution rates of the various species from the volcanic glass to vary with pH of the aqueous phase. The thermodynamic data base employed for these calculations contained data for 223 minerals, 293 aqueous complexes, and 14 solid solutions. These totals include the zeolite data discussed in the following section. Most of the mineral data and much of the aqueous-complex data are from compilations by Helgeson et al. (1970) and Helgeson et al. (1978). Most of the solid solutions are treated as ideal solutions; this is certainly an approximation, but it is generally necessary because of a lack of data. The Appendix contains a list of compositions of the minerals and solid-solution end members referred to in this paper, as defined in the EQ3/6 data base. Calculations were done at temperatures from 25 to 175°C because temperature was considered one of the important parameters in this analysis. Thermodynamic data are available from 0 to 300°C for most species in the EQ3/6 data base; however, the volcanic-glass dissolution rates measured at 25°C were used in all calculations. Although absolute dissolution rates should increase rapidly with increasing temperature, the relative rates used in the reaction-path calculation would be affected much less by temperature. Calculations and thermodynamic data are for a total pressure of 1 atm up to 100°C and for the saturation pressure of water at higher temperatures.

III. ZEOLITE THERMODYNAMIC DATA ESTIMATES

Zeolites, with silica and clays, form much of the alteration products observed at Rainier Mesa and other NTS locations. Thus, to model mineral formation in these areas, these minerals should be included in the thermodynamic data base. Of the three zeolites in the normal EQ3/6 data base

(laumontite, wairakite, and analcime), only analcime has been observed at NTS. No thermodynamic data were found for three other zeolites regularly observed at NTS: clinoptilolite, heulandite, and mordenite (White et al. 1980; Waters and Carroll 1981; Caporuscio et al. 1982). Thus, data have been estimated for these zeolites so that they may be considered as potential precipitates.

The first problem to be faced with zeolites is specification of a chemical formula. Zeolites labeled clinoptilolite, heulandite, and mordenite have been observed with varying composition, particularly, the silicon/aluminum ratio and the exchangeable cation composition (Sykes et al. 1979; Caporuscio et al. 1982; Smyth and Caporuscio 1981). Indeed, these zeolites are best described as having a relatively fixed aluminosilicate framework to which exchange cations (normally sodium, potassium, calcium, and magnesium) are more loosely bound. For these calculations, each zeolite was considered to be a solid solution with respect to the exchange cations. EQ3/6 treats solid solutions by defining a set of end members that compose the solid solution and mixing these end members in varying proportions to achieve the desired composition. For estimation purposes, a set of pure-component zeolites has been defined that approximates the silicon/aluminum ratios of clinoptilolite, heulandite, and mordenite found at NTS and other locations (Smyth and Caporuscio 1981; Mumpton 1977). For clinoptilolite, all four exchange cations have been observed. Few data are available on mordenite; only sodium and potassium are normally seen. For heulandite, calcium and traces of magnesium have been found; only the calcium form was considered. Table I lists the chemical formulae employed for these estimations.

To add these zeolites to the EQ3/6 data base, the thermodynamic data needed are the equilibrium constants (K_f) for the formation reactions for the zeolites from the aqueous basis set used in EQ3/6. As an example, the formation reaction for sodium-clinoptilolite is

$$2Na^+ + 2Al^{3+} + 10SiO_2(aq) + 12H_2O = Na_2[Al_2Si_{10}O_{24}]\cdot 8H_2O + 8H^+ \quad .$$

The quantity $\log_{10} K_f$ can be calculated from the free energy of formation of the mineral from the elements in their standard states (ΔG_f^o). Three methods of estimating ΔG_f^o were considered for use here: Tardy and Garrels (1974), Nriagu (1975), and Chen (1975). Of the three, the methods proposed by Tardy and Garrels and by Nriagu have only been used with clay minerals and can

TABLE I

ZEOLITE FORMULAE

Clinoptilolite	Mordenite
$Na_2[Al_2Si_{10}O_{24}]\cdot 8H_2O$	$Na[AlSi_5O_{12}]\cdot 3H_2O$
$K_2[Al_2Si_{10}O_{24}]\cdot 8H_2$	$K[AlSi_5O_{12}]\cdot 3H_2O$
$Ca[Al_2Si_{10}O_{24}]\cdot 8H_2O$	Heulandite
$Mg[Al_2Si_{10}O_{24}]\cdot 8H_2O$	$Ca[Al_2Si_7O_{18}]\cdot 6H_2O$

only be used at 25°C because they require special sets of thermodynamic data or correction constants that have been determined at that temperature only. Chen's method uses a sequence of reactions forming the mineral of interest from simpler compounds to estimate ΔG_f^o for the mineral. As long as ΔG_f^o data are available for the simpler compounds as a function of temperature, Chen's method can be used at any temperature. Because of its flexibility, the method proposed by Chen was used for the zeolite estimates reported here.

A group of minerals for which thermodynamic data are available in the range 0 to 300°C, and which can be used as the simpler compounds in Chen's method for these zeolites, is available in the EQ3/6 data base. These minerals, supplemented by data for Na_2O, K_2O, CaO, and MgO from the SUPCRT compilation (Helgeson et al. 1978), were used (see list in Table II). An advantage of using data from the EQ3/6 data base for estimations is that it provides zeolite data that are consistent with the other thermodynamic data employed in the reaction-path calculations. Values of $\log_{10} K_f$ for formation reactions from the EQ3/6 basis species were available as a function of temperature for all the species listed in Table II. Rather than converting these data to ΔG_f^o data, doing the estimation, and converting the results back to $\log_{10} K_f$ data, the equivalent procedure of estimating $\log_{10} K_f$ data for the zeolites directly from $\log_{10} K_f$ data for the simpler compounds was used. In other respects, Chen's method was used as originally proposed. Estimates were made at 0, 25, 60, 100, 150, 200, 250, and 300°C. Figures 2 and 3 show plots of $\log_{10} K_f$ as a function of temperature for the seven pure-component zeolites listed in Table I.

It is difficult to judge the accuracy of these estimates. As a test of the method and data, estimates were also made of $\log_{10} K_f$ for $CaAl_2Si_4O_{12}\cdot 2H_2O$

TABLE II

SIMPLE COMPOUNDS USED TO ESTIMATE ZEOLITE FORMATION CONSTANTS BY CHEN'S METHOD

H_2O	CaO
SiO_2(quartz)	$CaSiO_3$(wollastonite)
Al_2O_3(corundum)	$CaAl_2SiO_6$(Ca-Al pyroxene)
Al_2SiO_5(kyanite)	$CaAl_2SiO_8$(anorthite)
K_2O	$Ca_2Al_2SiO_7$(gehlenite)
$KAlSiO_4$(kalsilite)	$CaAl_2Si_4O_{12}\cdot 2H_2O$(wairakite)
$KAlSi_3O_8$(K-feldspar and high sanidine)	$CaAl_2Si_4O_{12}\cdot 4H_2O$(laumontite)
Na_2O	$CaAl_2Si_3O_{10}(OH)$(prehnite)
$NaAlSiO_4$(nepheline)	$CaAl_2Si_3O_{12}$(zoisite)
$NaAlSi_3O_8$(low albite and high albite)	$CaAl_2(Al_2Si_2O_{10})(OH)_2$(margarite)
$NaAlSi_2O_6$(jadeite and dehydrated analcime)	MgO
$NaAlSi_2O_6\cdot H_2O$(analcime)	$MgSiO_3$(enstatite)
	$MgAl_2O_4$(spinel)

(wairakite) and $NaAlSi_2O_6\cdot H_2O$ (analcime) by using data for other minerals listed in Table II. For wairakite, for example, data for quartz, corundum, kyanite, CaO, wollastonite, Ca-Al pyroxene, and anorthite were used. Table III compares the estimates with EQ3/6 data and other sources for these minerals (Robie et al. 1979; Plummer et al. 1976). Differences between the estimates and data from the compilations are of the same order as differences among the compilations. Unfortunately, Chen's method does not distinguish between polymorphs; also, although it gives different values of ΔG_f^o for minerals with the same structure but different quantities of hydration water, the $\log_{10} K_f$ for these minerals is the same. Thus, the same $\log_{10} K_f$ would be estimated for wairakite and laumontite, and the same $\log_{10} K_f$ would be estimated for analcime, dehydrated analcime, and jadeite.

IV. RESULTS

The results of the reaction-path calculations include an aqueous-phase composition and a list of minerals (identity and quantity) in equilibrium with the aqueous phase under the constraints of the calculation as a function of

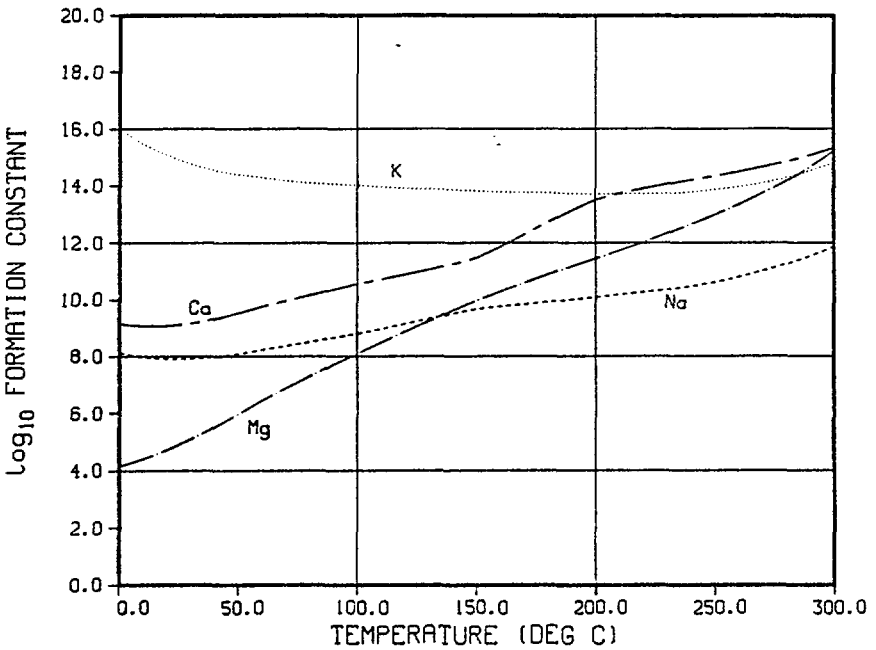

Fig. 2. Clinoptilolite formation constants.

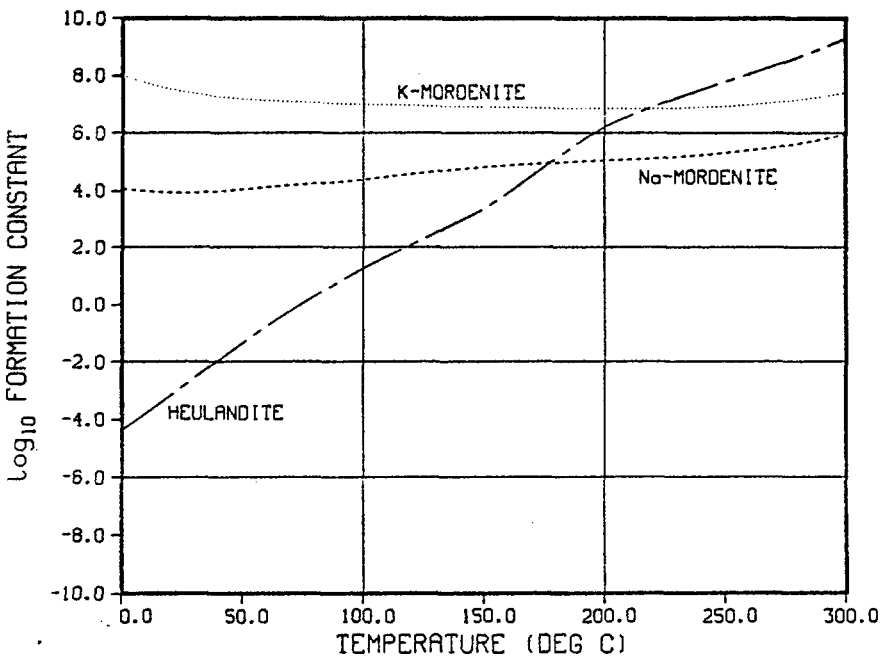

Fig. 3. Mordenite and heulandite formation constants.

TABLE III

COMPARISON OF ESTIMATED AND LITERATURE VALUES FOR WAIRAKITE AND ANALCIME FORMATION CONSTANTS

	$Log_{10} K_f$	
Wairakite	25°C	300°C
Estimate	-20.52	+1.42
EQ3/6	-18.56	+2.73
WATEQF[a]	-17.40	-
Analcime		
Estimate	-7.57	+0.39
EQ3/6	-7.28	+0.15
WATEQF[a]	-9.35	-
Robie et al. 1979	-6.73	-

[a]Plummer et al. 1976.

the reaction-progress variable. The reaction-progress variable is a measure of the extent of glass dissolution; specifically, for these calculations, it is the number of moles of SiO_2(aq) dissolved from the glass per kilogram of water in the aqueous phase. The calculated results will be compared with Rainier Mesa water compositions as reported by White et al. (1980). In particular, Na^+, K^+, Ca^{2+}, Mg^{2+}, and SiO_2(aq) contents, in addition to pH, will be discussed. Predicted mineral precipitates will also be compared with observed minerals at Rainier Mesa and other NTS locations. The general procedure followed here was to define a small number of cases in which precipitation of certain minerals (in one case none) was suppressed. Reaction-path calculations were done for each case at one or more temperatures and also for various Al^{3+} and Fe^{3+} dissolution rates. The calculated mineral assemblages and water compositions for each case were discussed and compared with observations.

The values of pH reported for the calculations are at temperature, whereas the measured values were taken at approximately 25°C. The effect of changing temperatures in the 25 to 175°C range on the pH of the solutions discussed here is small (less than 0.2 pH units) for values of pH less than 7. Solutions of pH 8 to 9 at temperature will increase in pH by 0.3 to 0.5 pH units when

they cool to 25°C. The change in pH of these solutions with temperature is a second-order effect and will be neglected in discussing the results of the calculations.

The general trend of the results is the same for all cases. In early stages of the reaction path (reaction progress $<\sim 10^{-4}$), aqueous-phase composition is controlled by the dissolution process; few or no precipitates have formed. Solution pH starts at 4.5, the pH assumed for the initial glass-free carbonate solution, and it increases with increasing reaction progress. In intermediate stages ($\sim 10^{-4}$ < reaction progress $<\sim 10^{-1}$), various minerals precipitate and begin to control the aqueous-phase composition. In the latter stages of the reaction path (reaction progress $>\sim 10^{-1}$), a stable mineral assemblage has formed that controls the aqueous-phase composition. Solid-solution compositions in the mineral assemblage and the aqueous-phase composition change slowly with increasing reaction progress, approaching a steady-state condition, where the aqueous-phase composition is constant and the dissolution rate of each species equals the rate of accumulation of that species in the mineral assemblage. All calculations were run to a reaction progress of at least 0.2. By this time, a stable mineral assemblage had usually formed, although compositions of solid solutions, and thus the aqueous phase, were still changing slowly with increasing reaction progress. Calculations were run to a reaction progress of 0.4 to 0.8 in a few cases where obvious changes were still occurring at 0.2 and in a few other cases to test the stability of the mineral assemblage.

A. No Precipitates Suppressed

The first calculations done suppressed none of the minerals in the data base. Figure 4 shows a plot of aqueous-phase pH as a function of reaction progress for calculations at 25, 75, and 125°C. The pH starts at 4.5 and rises to 8 to 10, where it is controlled by the mineral assemblage. The pH of Rainier Mesa water is generally in the range of 7 to 8. Thus, the predicted mineral assemblage in this case results in a solution pH that is higher than observed, although as temperature increases, solution pH is decreasing toward the observed range. At pH 7, the total dissolved silica content of the aqueous phase is 0.1 mmolal at 25°C, 0.5 mmolal at 75°C, and 1.3 mmolal at 125°C; at 25 and 75°C, this is below the 0.7 to 1.3 mmolal range observed for Rainier Mesa water. Figure 5 shows a plot of total sodium, potassium, calcium, and magnesium content of the aqueous phase as a function of reaction progress at

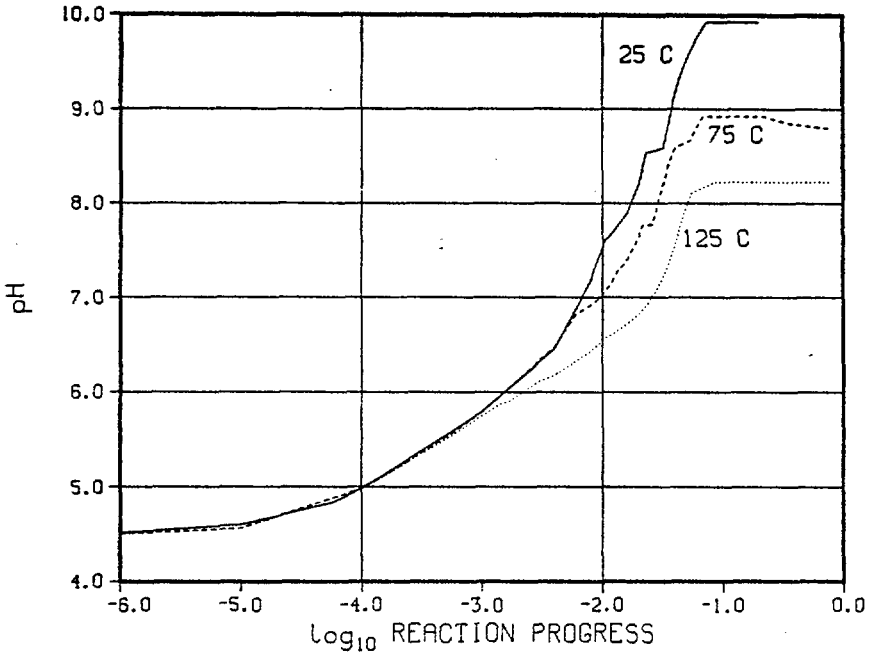

Fig. 4. Aqueous-phase pH. No mineral precipitates suppressed.

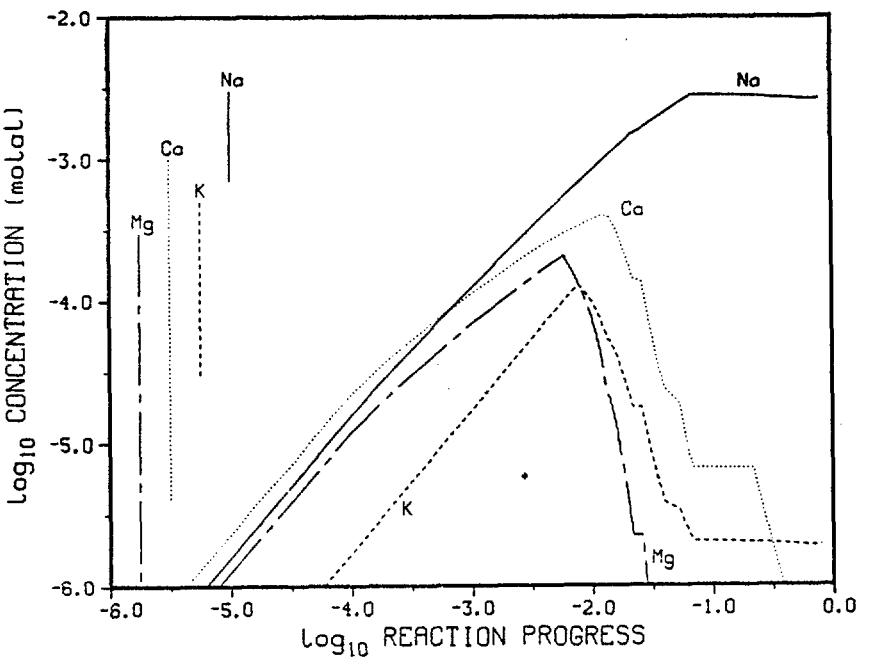

Fig. 5. Total sodium, potassium, calcium, and magnesium content of the aqueous phase at 75°C. No mineral precipitates suppressed. Vertical lines at left show ranges observed at Rainier Mesa.

75°C. The vertical lines at the left side of the figure represent ranges observed for these species at Rainier Mesa (White et al. 1980).

Another way to compare the alkali metal and alkaline earth compositions of the aqueous phase with observations is with a ternary diagram. Figure 6 shows the relative Na-K-Ca compositions at 25, 75, and 125°C on a ternary diagram. The line for each temperature represents the entire reaction path from the start (40% sodium, 57% calcium, and 3% potassium) to a reaction progress of 0.2 or greater (essentially all sodium). The shaded area represents the range of relative composition observed at Rainier Mesa (White et al. 1980). At the start of the reaction-path calculation, the relative compositions at all temperatures are essentially the same, being dominated by the dissolution rates of these species from the glass. As reaction progress increases, the relative sodium content steadily increases, the relative calcium content steadily decreases, whereas the relative potassium content remains in the 0 to 15% range. The reaction paths at 25 and 75°C remain on the low-potassium side of the observed range, but at 125°C, the reaction path agrees with observations. A similar plot for relative Na-K-Mg compositions shows that the 25°C reaction path also remains on the low-potassium side of the observed range, but the higher temperature reaction paths agree well with observations. The trend of both relative-composition plots with increasing reaction progress, that is, toward the sodium apex, is the same as the trend of observations on interstitial water with increasing depth at Rainier Mesa (White et al. 1980). Thus, the shaded areas near the sodium apex represent the deepest interstitial water compositions, whereas the shaded regions farthest from the sodium apex represent the shallowest compositions.

Figure 7 shows a plot of the total quantities of the various minerals precipitated (moles per kilogram of water in the aqueous phase) at 75°C as a function of reaction progress. In addition to those present in the final mineral assemblage, some minerals precipitate and redissolve as reaction progress increases. Two minerals that precipitate and redissolve in the reaction-progress range 10^{-2} to 10^{-1} and are not shown in Fig. 7 because of crowding are calcite ($<4 \times 10^{-4}$ moles/kg water) and dolomite ($<3 \times 10^{-5}$ moles/kg water). At 25°C, the final mineral assemblage contains quartz, kaolinite, sodic muscovite, nontronite, paragonite, calcite, and saponite; hematite and dolomite precipitate and redissolve during the calculation. At 125°C, the final mineral assemblage contains quartz, beidellite, saponite,

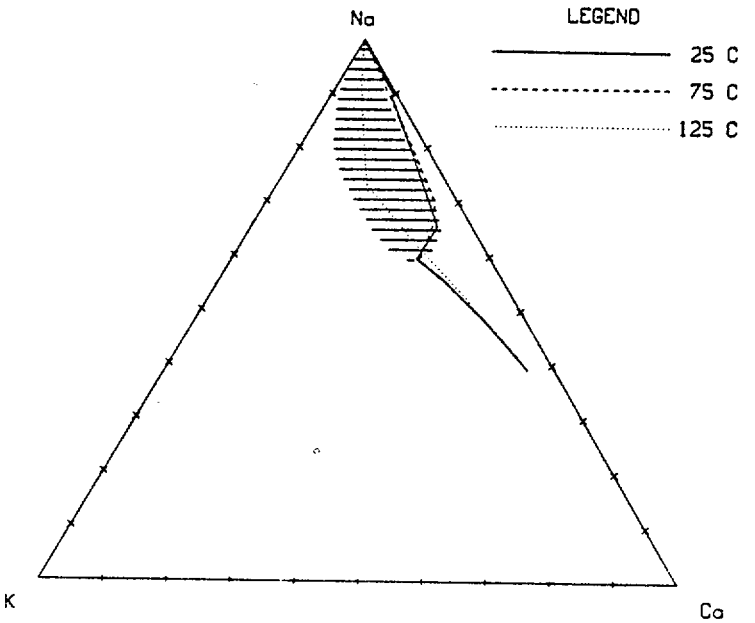

Fig. 6. Relative Na-K-Ca content of the aqueous phase. No mineral precipitates suppressed.

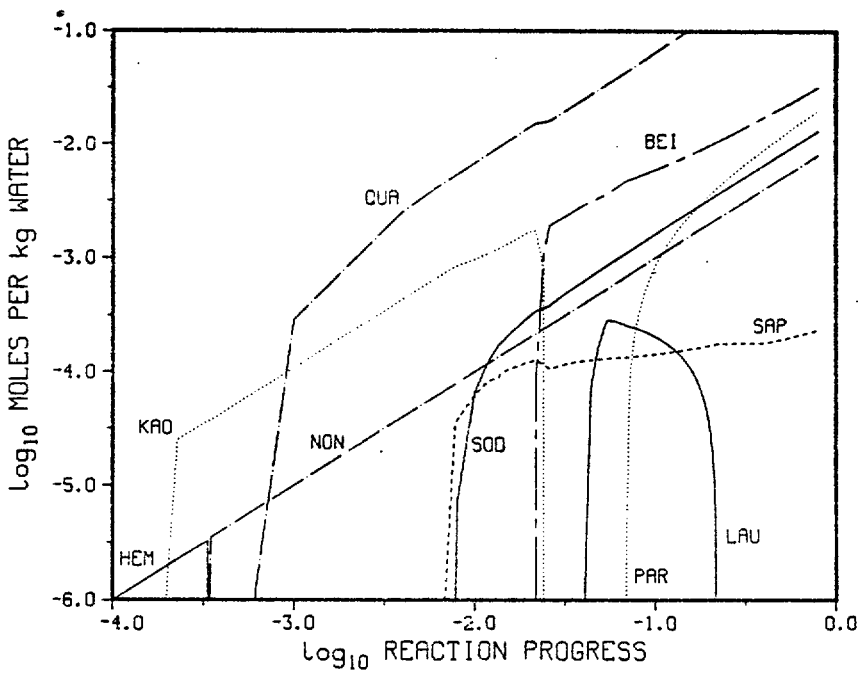

Fig. 7. Mineral precipitates at 75°C. No mineral precipitates suppressed. Mineral abbreviations listed in Appendix.

nontronite, plagioclase, and sodic muscovite; hematite, calcite, and prehnite precipitate and redissolve during the calculation. None of the zeolites observed at Yucca Mountain are part of the mineral assemblages for this case.

Doubling or halving the Al^{3+} dissolution rate had little effect on the results at 75°C. Solution pH and total dissolved silica content remain about the same. The identity of minerals in the final solid-phase assemblage is also generally the same. With a low Al^{3+} dissolution rate, more quartz and less clay precipitates, and plagioclase precipitates at a reaction progress of $\sim 10^{-1}$. With a high Al^{3+} dissolution rate, more clay and less quartz precipitates. Varying the Fe^{3+} dissolution rate mainly affects precipitation of nontronite, an iron-rich smectite clay. Essentially all the iron from the volcanic glass precipitates in this form. The results for the aqueous phase are essentially unaffected by changes in the Fe^{3+} dissolution rate.

None of the mineral assemblages predicted for this case contain the zeolites clinoptilolite or mordenite that have been observed at Rainier Mesa and other NTS locations. Also, the dissolved silica content of the aqueous phase is lower than observed for Rainier Mesa water except at 125°C. Because cristobalite rather than quartz is usually associated with clinoptilolite and mordenite, it may be necessary to have a higher SiO_2(aq) activity to precipitate these zeolites. This question is investigated in the following section.

B. Quartz and Chalcedony Precipitation Suppressed

A number of calculations were done in which precipitation of quartz and chalcedony was suppressed to increase SiO_2(aq) activity. In addition, precipitation of nontronite was suppressed in most of these calculations to control the clay precipitate composition. Figure 8 shows a plot of aqueous-phase pH for runs at 25, 75, 125, and 175°C, in which precipitation of quartz, chalcedony, and nontronite was suppressed. The final values of pH, where the system is controlled by the solid-phase assemblage, are from 7 to 8.5; the results from the 75, 125, and 175°C calculations are in the range observed at Rainier Mesa. At pH 7, the total dissolved silica content is 0.36 mmolal at 25°C, 1.32 mmolal at 75°C, 3.1 mmolal at 125°C, and 5.8 mmolal at 175°C. Thus, the 75°C result agrees best with the range observed at Rainier Mesa (0.7 to 1.3 mmolal). Higher temperature conditions could also be in agreement with observed silica content if it is assumed that some solid silica precipitation occurs as a sample is cooled to room temperature.

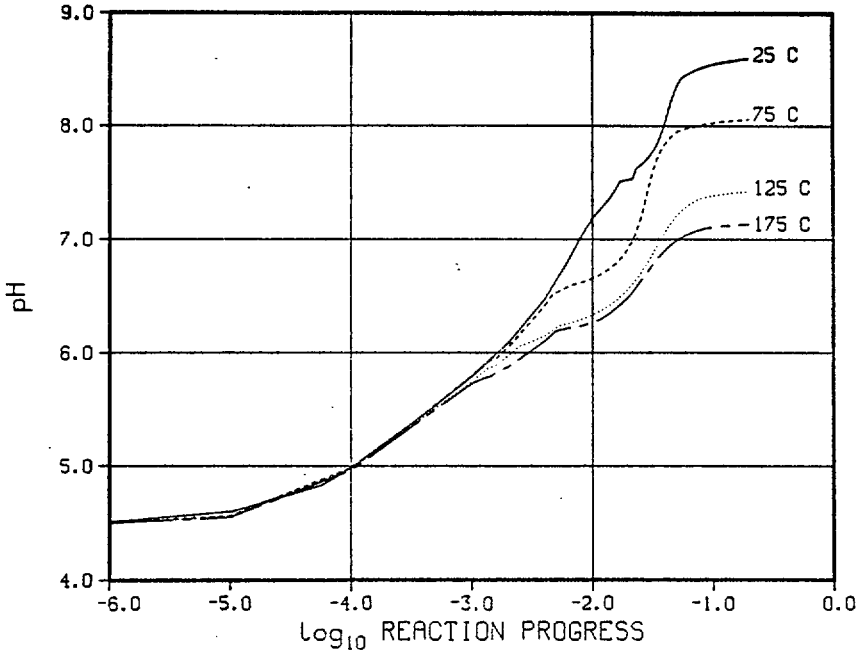

Fig. 8. Aqueous-phase pH. Precipitation of quartz, chalcedony, and nontronite suppressed.

Figure 9 shows a plot of total sodium, potassium, calcium, and magnesium content of the aqueous phase as a function of reaction progress for the 75°C calculation. The vertical lines at the left represent ranges observed for these species at Rainier Mesa. The calcium and potassium concentrations drop below the observed ranges toward the end of the calculation. Figure 10 shows a similar plot for the 125°C run; the final calcium and potassium concentrations are higher in this calculation and closer to the observed ranges.

Figure 11 shows the relative Na-K-Ca compositions at 25, 75, 125, and 175°C. At the start of the reaction-path calculation, the relative compositions at the four temperatures are essentially the same, being dominated by the dissolution rates of these species from the glass. At about the time the reaction paths enter the observed range of relative compositions (shaded area), the reaction-progress variable is in the range 10^{-3} to 10^{-2}; the reaction paths at the four temperatures begin to separate as precipitation starts, and the solid-phase assemblages begin to influence the aqueous phase. At later values of the reaction-progress variable ($>10^{-2}$), all four reaction paths approach the sodium apex along different paths. The 25°C reaction path skirts the edge of the observed area, with too little potassium. The 75 and 125°C reaction paths show the best agreement with observed compositions. The 175°C

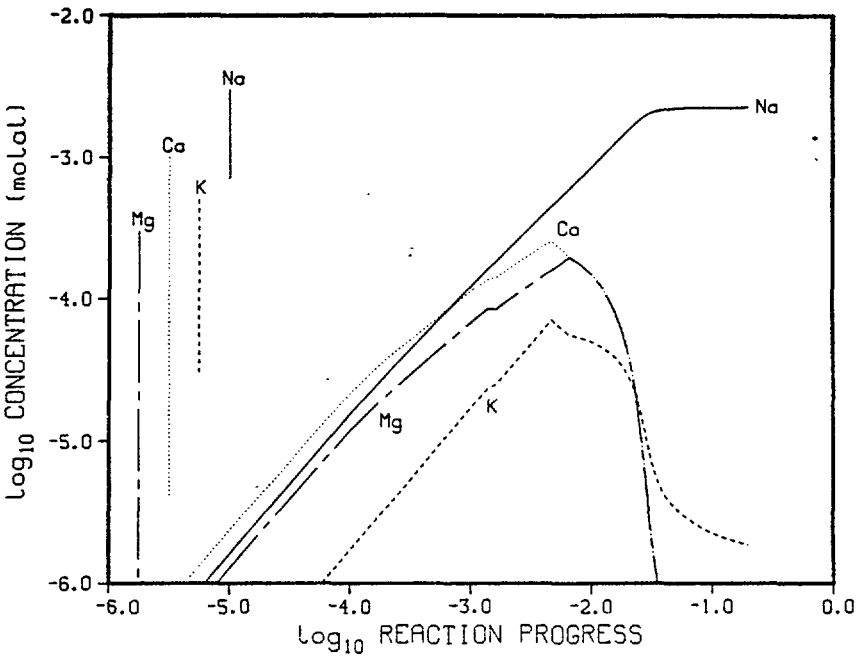

Fig. 9. Total sodium, potassium, calcium, and magnesium content of the aqueous phase at 75°C. Precipitation of quartz, chalcedony, and nontronite suppressed. Vertical lines at left show ranges observed at Rainier Mesa.

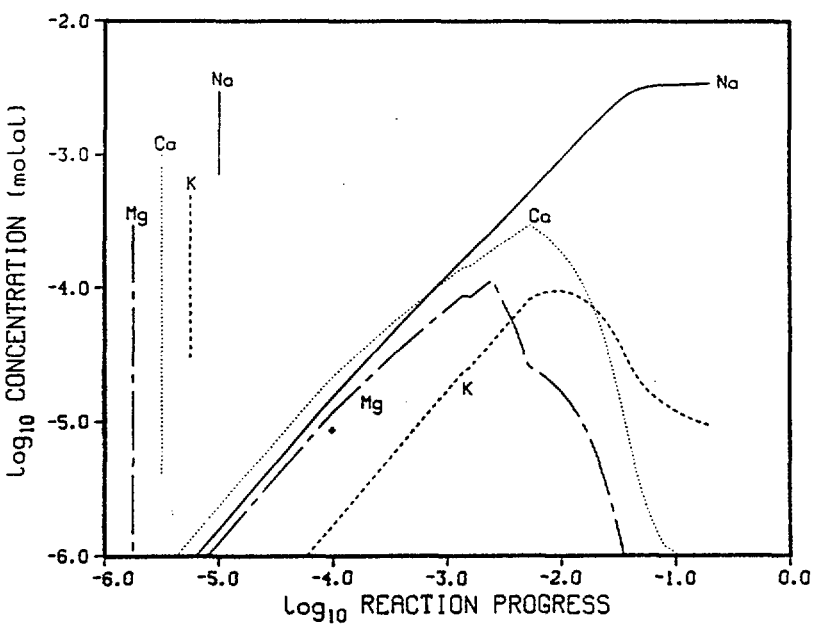

Fig. 10. Total sodium, potassium, calcium, and magnesium content of the aqueous phase at 125°C. Precipitation of quartz, chalcedony, and nontronite suppressed. Vertical lines at left show ranges observed at Rainier Mesa.

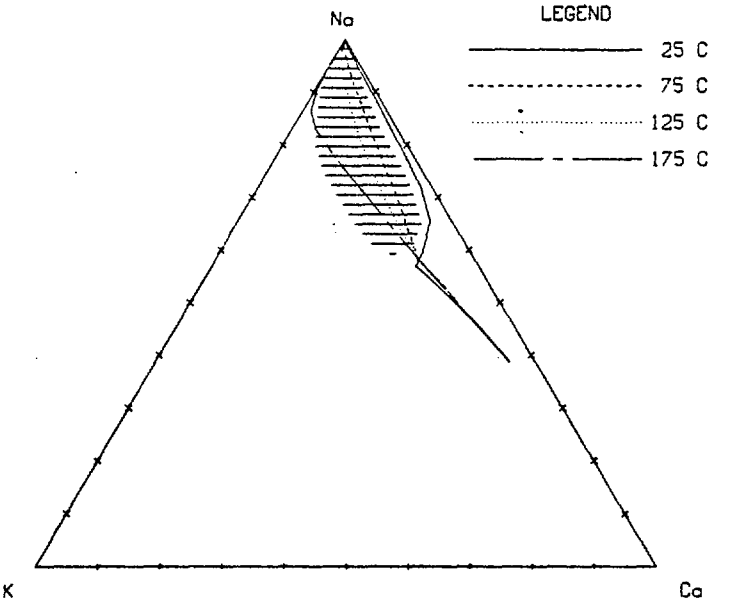

Fig. 11. Relative Na-K-Ca content of the aqueous phase. Precipitation of quartz, chalcedony, and nontronite suppressed.

reaction path shows too much potassium late in the reaction path. Figure 12 shows a similar plot of the relative Na-K-Mg composition of the aqueous phase. In this case, the 25°C reaction path also shows too little potassium, whereas the 75°C reaction path borders on the low-potassium side of the observations. The 125 and 175°C reaction paths show good agreement with the observations. As noted in the previous section, the trend with increasing reaction path is the same as the trend of interstitial water compositions with depth at Rainier Mesa.

The minerals in the final mineral assemblage are the same at each temperature: cristobalite, beidellite, clinoptilolite, mordenite, hematite, and saponite. The quantities differ and the compositions of the four solid solutions (beidellite, clinoptilolite, mordenite, and saponite) also differ. The composition differences in the solid solutions lead to the different aqueous-phase compositions calculated at the various temperatures. Figure 13 shows a plot of the total quantities of the various minerals precipitated as a function of reaction progress at 75°C. In addition to the minerals present in the final-phase assemblage, kaolinite forms early in the calculation but is replaced by beidellite; gibbsite forms early in very small quantities but

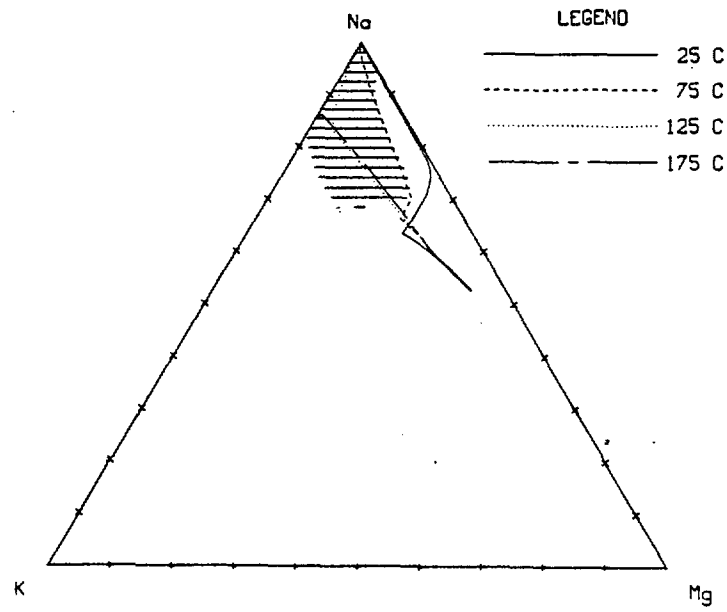

Fig. 12. Relative Na-K-Mg content of the aqueous phase. Precipitation of quartz, chalcedony, and nontronite suppressed.

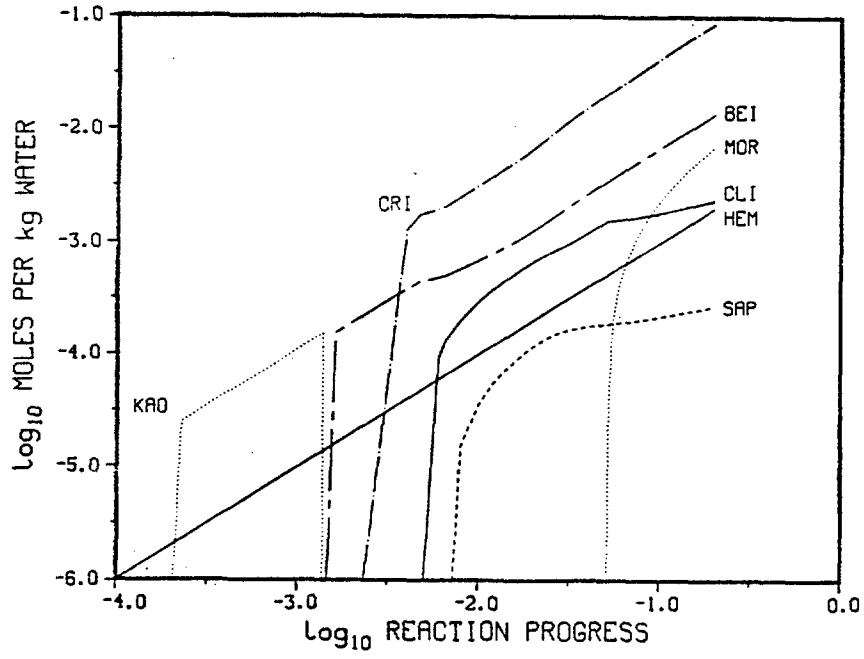

Fig. 13. Mineral precipitates at 75°C. Precipitation of quartz, chalcedony, and nontronite suppressed. Mineral abbreviations listed in Appendix.

redissolves as the silicon/aluminum ratio in the aqueous phase increases. The precipitation of clays (beidellite, and nontronite if it is not suppressed) before the zeolites is in agreement with observations (Hoover 1968; Moncure et al. 1981). Saponite does precipitate after clinoptilolite but before mordenite.

The zeolite clinoptilolite precipitates as a solid solution involving sodium, potassium, calcium, and magnesium end members (see Table I). The magnesium content of the clinoptilolite predicted to precipitate here is quite small. Figure 14 shows a plot of the relative Na-K-Ca content of the clinoptilolite precipitated for the 25, 75, 125, and 175°C calculations. The line for each temperature represents the entire reaction path; compositions start along the Ca-K boundary and move toward the sodium apex as reaction progress increases and the aqueous phase increases in sodium content (see Figs. 9 and 10). The single point at 22% sodium, 36% potassium, and 42% calcium is from an average clinoptilolite analysis at one depth at Rainier Mesa (White et al. 1980). The Rainier Mesa clinoptilolite has a significant amount of magnesium, whereas the compositions predicted here have essentially none. The trend from the K-Ca boundary toward the sodium apex is similar to a trend seen for zeolite (clinoptilolite plus mordenite) compositions with increasing depth at Yucca Mountain (Caporuscio et al. 1982). However, the Yucca Mountain zeolites show higher sodium content than was calculated here. The other zeolite predicted to precipitate here is mordenite. It involves only sodium and potassium end members and precipitates late in the calculation (see Fig. 13). Mordenite compositions range from ~50% sodium at 25°C to ~65% sodium at 175°C. If the relative Na-K-Ca content of clinoptilolite and mordenite was calculated as if the two zeolites were one mineral, the curves shown in Fig. 14 would be shifted toward the Na-K boundary after mordenite precipitates. This would bring the calculated results more into line with the observations at Yucca Mountain but not into complete agreement.

The two clay minerals that are predicted to precipitate are also solid solutions. Both beidellite and saponite are members of the smectite group of clays. Both have hydrogen, sodium, potassium, calcium, and magnesium end members. Over most of the reaction path, both clays are composed of 60 to 80% calcium and magnesium forms and 20 to 40% hydrogen, sodium, and potassium forms. Precipitation of nontronite, an iron-rich smectite clay, was suppressed for these calculations. If nontronite is allowed to precipitate, hematite

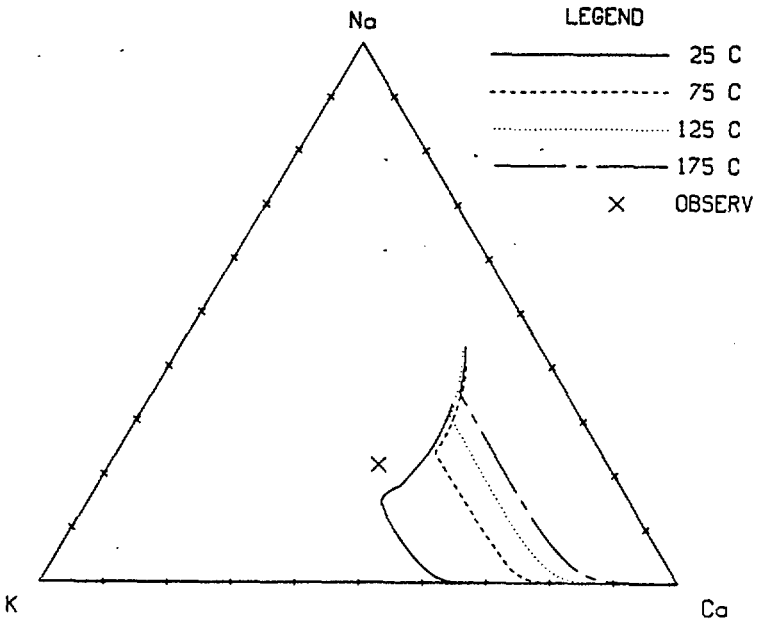

Fig. 14. Relative Na-K-Ca content of clinoptilolite precipitate. Precipitation of quartz, chalcedony, and nontronite suppressed. The x locates the average clinoptilolite composition observed at Rainier Mesa.

still precipitates initially, but it is replaced early in the reaction path by nontronite as the iron-bearing mineral. The remainder of the phase assemblage, including the presence of beidellite, is essentially the same as when nontronite precipitation is suppressed; there are small changes in the quantities of other minerals and compositions of other solid solutions to account for the presence of nontronite. Thus, the reaction-path calculations indicate that iron will precipitate in smectite clays or, if the kinetics of clay precipitation are too slow, as hematite.

Doubling the Al^{3+} dissolution rate in the case where precipitation of quartz and chalcedony is suppressed has little effect on the aqueous-phase results at 75°C. In the final solid-phase assemblage, the quantities of cristobalite and clinoptilolite were reduced, whereas the quantity of beidellite was increased. Saponite precipitated initially at about the same value of reaction progress, but it redissolved before the end of the calculation. Reducing the Al^{3+} dissolution rate by half at 75°C also has little effect on the aqueous-phase results. The minerals precipitated are the same as those with the nominal Al^{3+} dissolution rate; the quantities of cristobalite and clinoptilolite are increased and the quantity of beidellite

is reduced. Increasing or decreasing the dissolution rate of Fe^{3+} alters the amount of hematite or nontronite precipitate in a like manner; it has essentially no other effects.

Suppressing precipitation of quartz and chalcedony to increase SiO_2(aq) activity has produced water compositions that are in good agreement with observations of Rainier Mesa. The mineral assemblages predicted are also in good agreement with the first stage of mineral evolution at NTS, a cristobalite, smectite clay, zeolite mixture (Moncure et al. 1981). The best agreement was obtained for water temperatures in the 75 to 125°C range. Increasing SiO_2(aq) activity further by also suppressing precipitation of cristobalite is pursued in the following section.

C. Quartz, Chalcedony, and Cristobalite Precipitation Suppressed

The SiO_2(aq) activity can be increased further by suppressing precipitation of cristobalite, in addition to quartz and chalcedony. The only solid silica phase left in the data base is amorphous silica. Reaction-path calculations were done for this case (also suppressing nontronite precipitation) at 25, 75, and 125°C. The aqueous-phase pH attained with the stable mineral assemblage was well below that in the previous case when only quartz and chalcedony precipitation was suppressed; the final pH was 6.6 at all three temperatures. Thus, it is below the range observed for Rainier Mesa water (7 to 8). The total dissolved silica content of the aqueous phase is 1.9 mmolal at 25°C, 3.8 mmolal at 75°C, and 6.0 mmolal at 125°C. These concentrations are above the range observed at Rainier Mesa (0.7 to 1.3 mmolal). The total sodium, potassium, and calcium concentrations in the aqueous phase are similar to the results shown when only quartz and chalcedony precipitation was suppressed (see Figs. 9 and 10); however, magnesium concentrations are quite high at 25 and 75°C, and the reaction-path line remains well outside the observed area on a Na-K-Mg ternary diagram.

The stable mineral assemblage differs slightly at the three temperatures. At 25°C, hematite, the clay pyrophyllite, and the zeolite clinoptilolite precipitate. At 75°C, beidellite is added to the stable mineral assemblage. At 125°C, saponite replaces pyrophyllite. Amorphous silica is not one of the predicted precipitates; thus, the SiO_2(aq) activity is controlled by the clay and zeolite minerals. The high magnesium concentrations in the aqueous phase at 25 and 75°C are probably caused by the lack of saponite as a precipitate.

In this case, reducing the relative Al^{3+} dissolution rate from the glass to half its nominal value has a significant effect. At 75°C, amorphous silica now precipitates, and talc replaces pyrophyllite and beidellite as clay precipitates. The zeolites clinoptilolite and mordenite are also in the stable mineral assemblage. The pH of the aqueous phase increases to 7.2, which is within the observed range for Rainier Mesa water. However, the total dissolved silica content of the aqueous phase is still quite high (4.6 mmolal), and the magnesium content of the aqueous phase is also high. Doubling the Al^{3+} dissolution rate for this case merely leads to more clay precipitates with essentially no other effects. Increasing or decreasing the Fe^{3+} dissolution rate modifies the amount of hematite or nontronite precipitate in a like manner but has few other effects.

Agreement between calculated and observed water compositions and mineral assemblages is not as good in this case as in the previous one, where only quartz and chalcedony precipitation was suppressed. By reducing the Al^{3+} dissolution rate, agreement was improved somewhat; however, the total dissolved silica and magnesium contents of the aqueous phase are still too high.

D. Precipitation of Albite and Analcime

Results from calculations discussed in the previous sections have shown the formation of cristobalite, smectite clays, and the zeolites clinoptilolite and mordenite from dissolution of volcanic glass by using a simple reaction-path model. However, this is only the first stage in the mineral evolution scheme that has been proposed for NTS (Hoover 1968; Moncure et al. 1981; Waters and Carroll 1981). Further evolution leads to mineral assemblages that contain analcime and then albite. The steps in this sequence have been related to zones of increasing temperature (Iijima 1978). However, the reaction-path calculations in which precipitation of quartz and chalcedony was suppressed indicated that the same cristobalite, smectite, and zeolite mixture was stable up to 175°C, well above the temperature at which further steps in the sequence have been seen in field observations. The fact that $SiO_2(aq)$ activity had to be maintained higher than quartz equilibrium to achieve this mineral assemblage indicates that $SiO_2(aq)$ activity may be a controlling variable. This does not contradict observations pointing to temperature because increasing temperature may be related to faster quartz precipitation kinetics and a decrease in $SiO_2(aq)$ activity. In fact, the total dissolved silica

content of Rainier Mesa water decreases with increasing depth, which should correspond to increasing temperature (White et al. 1980).

Reaction-path calculations were done in an attempt to define the conditions under which albite and analcime would be in the stable mineral assemblage that results from volcanic-glass dissolution at Rainier Mesa. The reaction-path calculation in EQ3/6 is not now structured so that formation constants can be made a function of the reaction-progress variable. Thus, it was not possible to vary the SiO_2(aq) activity in a continuous fashion between the high value in equilibrium with cristobalite and the lower value in equilibrium with quartz. To determine what minerals would finally precipitate if the SiO_2(aq) activity were lower, complete reaction-path calculations were run in which quartz was allowed to precipitate; in fact, they are identical to the calculations first discussed in which nothing was suppressed. At 25 and 75°C (Fig. 7), no analcime or albite precipitates. However, at 125°C, plagioclase, a solid solution containing albite, is part of the final mineral assemblage, in addition to quartz, clay, and mica. Plagioclase can also be made part of the final mineral assemblage at 75°C by suppressing precipitation of the micas paragonite and sodic musconite (a solid solution containing paragonite). Figure 15 shows this mineral assemblage; it is similar to that in Fig. 7, except that plagioclase replaces paragonite, saponite redissolves, and kaolinite reprecipitates. As with Fig. 7, calcite and dolomite precipitate and redissolve in the reaction-progress range 10^{-2} to 10^{-1}, but they are not shown on Fig. 15 because of crowding. The aqueous phase accompanying the mineral assemblage in Fig. 15 is very similar to that shown in Figs. 4 through 6. In particular, the pH at the time plagioclase precipitates is 9, which is higher than the 7 to 8 range observed for Rainier Mesa water.

Another way to initiate the precipitation of albite without suppressing precipitation of any other minerals at 75°C is to reduce the Al^{3+} dissolution rate. Figure 16 shows a plot of minerals precipitated at 75°C as a function of reaction progress for an Al^{3+} dissolution rate half the nominal value. Both paragonite and plagioclase precipitate. In addition, saponite and laumontite do not redissolve, but beidellite does and is replaced by plagioclase. As with Figs. 7 and 15, calcite and dolomite are not shown in Fig. 16. The aqueous phase accompanying the mineral assemblage in Fig. 16 is also similar to that shown in Figs. 4 through 6, except that the aqueous

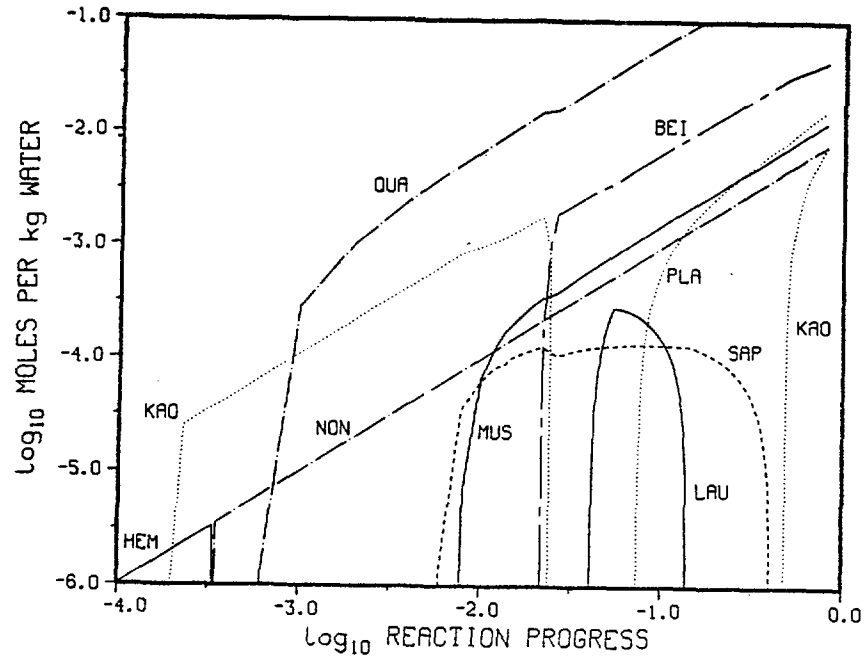

Fig. 15. Mineral precipitates at 75°C. Precipitation of paragonite and sodic muscovite suppressed. Mineral abbreviations listed in Appendix.

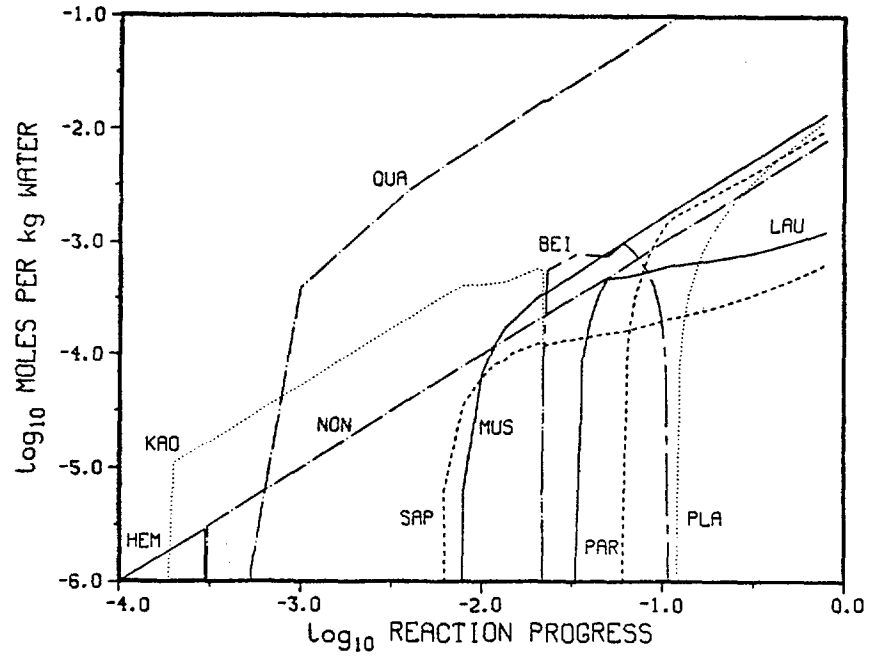

Fig. 16. Mineral precipitates at 75°C. No mineral precipitates suppressed. Al^{3+} dissolution rate from glass half the nominal value. Mineral abbreviations listed in Appendix.

calcium content remains higher at large values of the reaction progress in this case (see Fig. 5).

Three different sets of conditions have been defined in which albite is part of the final mineral assemblage; analcime was not found as a precipitate under any of these conditions. One set was suppression of precipitation of paragonite and sodic musconite at 75°C (see Fig. 15). If, in addition, precipitation of all albite minerals in the EQ3/6 data base is suppressed, the mineral assemblage shown in Fig. 17 is obtained. It is essentially the same as Fig. 15 except that analcime has replaced plagioclase, the solid solution containing albite. Thus, the reaction-path calculations show that if for some reason albite minerals do not precipitate under these conditions (slow precipitate kinetics, for example), analcime will be part of the final mineral assemblage.

The results of the reaction-path calculations in which albite or analcime precipitate have one common characteristic: SiO_2(aq) activity is low. This is in line with the observation that cristobalite, which implies a high SiO_2(aq) activity, is usually found with clinoptilolite and mordenite, and that quartz, which implies a lower SiO_2(aq) activity, is usually found with albite or analcime (Keith et al. 1978). The results further indicate that albite is the preferred precipitate. This can also be seen from a considera- tion of the reaction

$$\text{analcime} + \text{quartz} = \text{albite} + \text{water} \quad .$$

When data from the EQ3/6 data base are used, $\log_{10} K$ for this reaction is approximately +0.2 from 0 to 200°C. The three solid phases have unit activity, and the activity of water is very close to 1.0 in the dilute solutions and for the total pressures considered here. Thus, these data indicate albite is stable with respect to analcime (Helgeson et al. 1978). The same conclusion holds in the presence of other solid silica phases that are less stable than quartz. When other thermodynamic data are used, however, $\log_{10} K$ for this reaction was calculated as -0.15 at 25°C, indicating analcime is stable with respect to albite (Robie et al. 1979). Experimental studies also indicate that analcime is stable at low temperatures but that albite is stable at higher temperatures (Thompson 1971; Liou 1971). However, these experiments were done at pressures much greater than the saturation pressure of water, which is

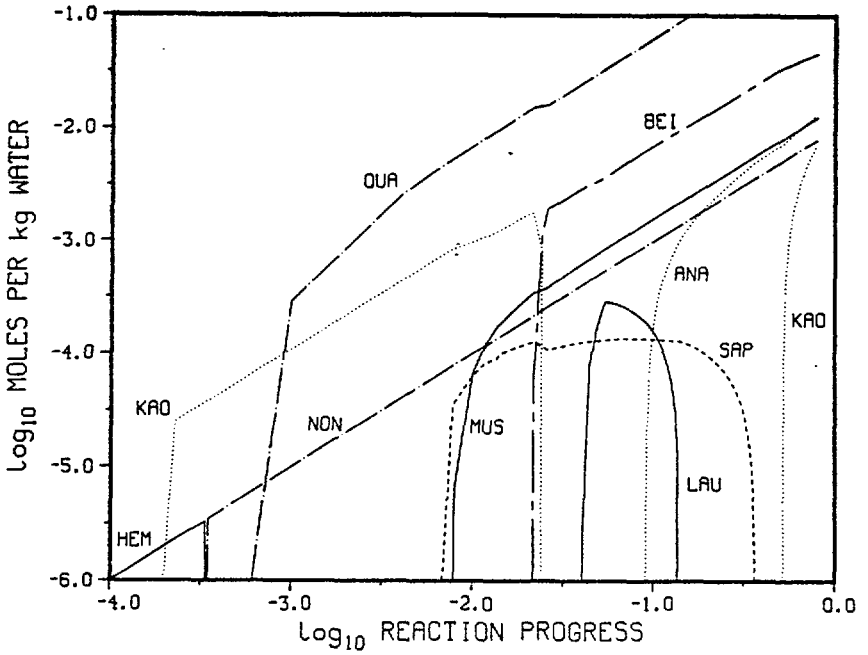

Fig. 17. Mineral precipitates at 75°C. Precipitation of paragonite, sodic muscovite, and all albite minerals suppressed. Mineral abbreviations listed in Appendix.

assumed in the calculations. At several kilobars pressure, the activity of water increases enough to drive the reaction to the left, making analcime stable with respect to albite at low temperatures (Helgeson et al. 1978). The relative stability of albite and analcime may thus be a function of total pressure, which was not considered as a variable here because of present limitations in EQ3/6.

E. Dissolution Rates Proportional to Relative Composition

So far, all the reaction-path calculations have used volcanic-glass dissolution rates based on the measurements of White et al. (1980) and assumed rates for Al^{3+} and Fe^{3+}. If dissolution-rate measurements had not been made, congruent dissolution would have been a logical assumption to use for these calculations. A reaction-path calculation was done at 75°C by using dissolution rates that are proportional to the relative composition of the glass (White et al. 1980) to see the effect this would have on the results. Table IV compares the dissolution rates based on composition with rates used previously at pH 5 and 7. The major differences occur with K^+, Ca^{2+}, and Mg^{2+}. Based on composition, K^+ has a much higher dissolution rate, and Ca^{2+} and Mg^{2+} have much lower rates than measurements indicate.

TABLE IV

VOLCANIC-GLASS DISSOLUTION RATES

Species	Rate Proportional to Composition	Rates from Fig. 1 pH = 5	pH = 7
Na^+	0.101	0.1437	0.0657
K^+	0.094	0.0170	0.0170
Ca^{2+}	0.0064	0.1758	0.0176
Mg^{2+}	0.0049	0.0994	0.0151
$SiO_2(aq)$	1.000	1.000	1.000
Al^{3+}	0.226	0.220	0.220
Fe^{3+}	0.020	0.020	0.020
OH^{-a}	0.9556	1.4311	0.8681

[a]OH^- rate set to maintain electrical neutrality.

For this calculation, precipitation of quartz, chalcedony, and nontronite was suppressed. Thus, the results should be compared with Figs. 8, 9, and 11 through 14. The pH is similar to the 75°C curve in Fig. 8 except that at a reaction progress of $\sim 10^{-1}$, the pH takes a sharp rise to 8.5, staying constant at that value until the end of the calculation. Figure 18 shows a plot of total sodium, potassium, calcium, and magnesium content of the aqueous phase as a function of reaction progress. The vertical lines at the left represent ranges observed for these species at Rainier Mesa. Early in the calculation (reaction progress $< \sim 10^{-3}$), before mineral phases begin to control aqueous-phase composition, the different dissolution rates lead to very different solution compositions (compare Figs. 9 and 18). Even after solid phases become important, the potassium content is higher and the calcium and magnesium contents are lower in this case. These differences are even more apparent in ternary diagrams. Figure 19 shows a plot of relative Na-K-Ca composition; it can be compared with the 75°C curve in Fig. 11. In this case, the high potassium dissolution rate leads to high potassium content of the aqueous phase. The reaction path starts at about 50% sodium and 50% potassium and moves toward the sodium apex, staying outside the observed range of

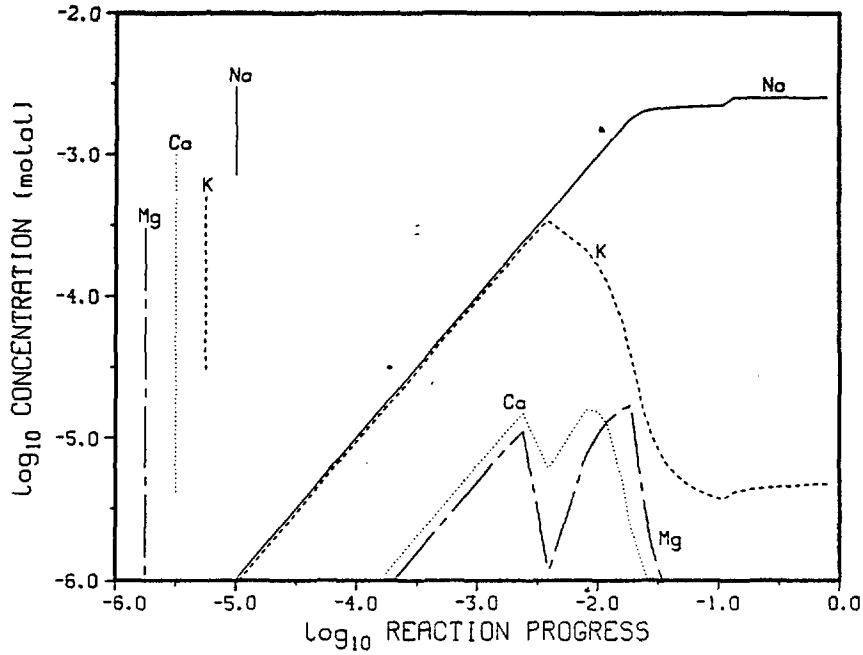

Fig. 18. Total sodium, potassium, calcium, and magnesium content of the aqueous phase. Precipitation of quartz, chalcedony, and nontronite suppressed. Congruent dissolution of volcanic glass.

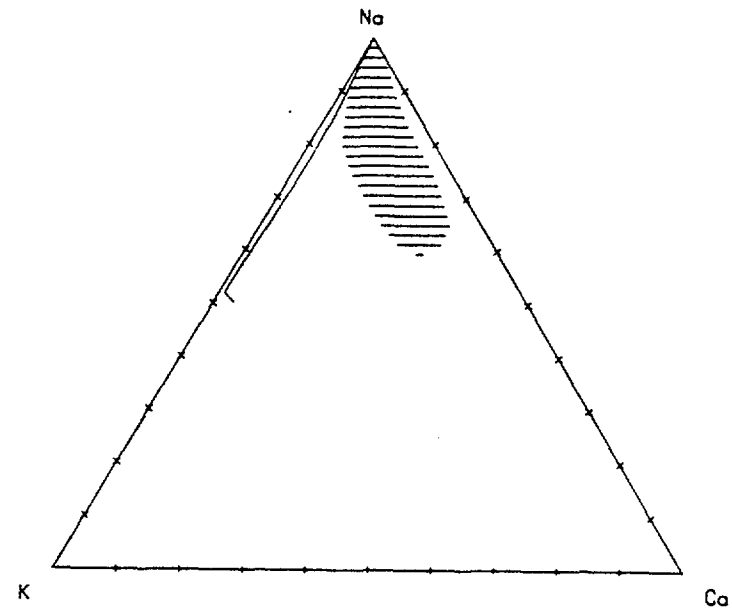

Fig. 19. Relative Na-K-Ca content of the aqueous phase. Precipitation of quartz, chalcedony, and nontronite suppressed. Congruent dissolution of volcanic glass.

compositions (shaded area) for most of the calculation. A plot of relative Na-K-Mg content is similar to Fig. 19.

Figure 20 shows a plot of the total quantities of the various minerals precipitated in this case as a function of reaction progress; it can be compared with Fig. 13, where measured dissolution rates were employed under these same conditions. The minerals precipitated are the same over most of the calculation; however, the precipitation order, the quantities, and the solid-solution compositions differ. In the reaction-progress range 0.1 to 0.15, cristobalite redissolves and albite precipitates; the pH of the aqueous phase rises from 8 to 8.5 over this range.

The largest differences between the results of this case and observations at Rainier Mesa are in the aqueous-phase composition (see Fig. 19). These differences are directly related to the high potassium and low calcium and magnesium dissolution rates that result from the assumption that congruent dissolution occurs. The results indicate that dissolution rates can have a significant effect on the aqueous and solid phases predicted by a reaction-path calculation.

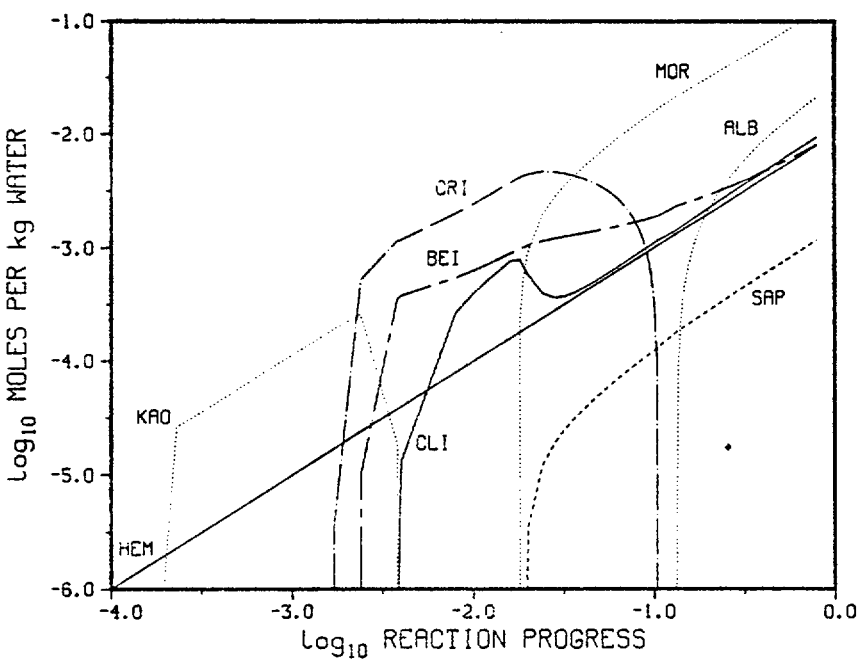

Fig. 20. Mineral precipitates at 75°C. Precipitation of quartz, chalcedony, and nontronite suppressed. Congruent dissolution of volcanic glass. Mineral abbreviations listed in Appendix.

V. SUMMARY AND DISCUSSION

This paper describes a reaction-path calculation of groundwater chemistry and mineral formation at Rainier Mesa. The calculation is based on a model proposed by Claassen and White (1978) in which water saturated with CO_2 reacts with volcanic glass. The various species composing the glass are leached or dissolved at different rates. Measured dissolution rates for $SiO_2(aq)$, Na^+, K^+, Ca^{2+}, and Mg^{2+} from Rainier Mesa glass were used; rates for Al^{3+} and Fe^{3+} were assumed. Groundwater chemistry is related to the relative dissolution rates of species from the glass and the minerals that precipitate during the dissolution process. The reaction-path calculation models this irreversible process as a sequence of equilibrium states in which relative dissolution rates control the total amounts of various species available; equilibrium thermodynamics is used to partition each species among the aqueous phase and possible mineral phases. Minerals that precipitate during the calculation remain in contact with the aqueous phase and can redissolve if conditions are appropriate. Precipitation of certain minerals was suppressed during some calculations to control aqueous-phase activities.

The EQ3/6 chemical equilibrium computer programs were used for these calculations. Although the thermodynamic data base for these programs is extensive, data for three zeolites found at NTS (clinoptilolite, heulandite, and mordenite) were not available. These data were estimated from 0 to 300°C by using the method proposed by Chen and thermodynamic data from the EQ3/6 data base.

The primary purpose of this work was to test whether equilibrium processes could be used to explain groundwater chemistry and minerals found at Rainier Mesa, Yucca Mountain, and other NTS locations. A number of qualitative discussions of zeolite formation have proposed the same general model, interaction of groundwater with volcanic glass, for this process (Hoover 1968; Moncure et al. 1981). Claassen and White (1978) made this model more quantitative by proposing a specific starting point and by measuring important rate processes involved in glass dissolution. This work makes the model still more quantitative by requiring that a reaction-path calculation be used to predict water composition and mineral precipitates. Although rate processes may control the availability of species through the dissolution process, the reaction-path calculation imposes equilibrium constraints at each step in the path and thus leaves little to the choice of the modeler. Of course, it is

naive to assume that only equilibrium processes can account for the Rainier Mesa system. Measured water compositions indicate supersaturation with respect to a number of minerals; quartz is one example. These supersaturations are usually attributed to kinetic constraints. Unfortunately, reaction-path programs are only beginning to consider kinetic limitations on such processes as precipitation. For this reason, the effects of slow kinetics, for example, supersaturation, were simulated by suppressing precipitation of certain minerals for a number of the calculations. For example, precipitation of quartz and chalcedony was suppressed to increase SiO_2(aq) activity, and precipitation of albite minerals was suppressed to allow analcime to precipitate. In cases where these constraints were necessary to match observations, equilibrium processes alone were not sufficient. Even though these constraints represent deviations from equilibrium behavior, as long as they are limited in nature and physically realistic, the overall model can still give useful quantitative results.

The first stage of mineral evolution, from volcanic glass to a cristobalite, smectite clay, and zeolite mixture, was modeled best by the reaction-path calculations with precipitation of quartz and chalcedony suppressed. The aqueous-phase pH and total dissolved silica, sodium, potassium, calcium, and magnesium content are all in the range observed at Rainier Mesa for calculations at 75 and 125°C (see Figs. 8 through 10). More important, the relative Na-K-Ca and Na-K-Mg compositions of the water move through the range of observed compositions on ternary diagrams as reaction progress increases (see Figs. 11 and 12). Also, the mineral assemblage contains cristobalite, the zeolites clinoptilolite and mordenite, and the smectite clays beidellite and saponite (see Fig. 13). The agreement between the calculated and observed mineral assemblage indicates that the estimated zeolite thermodynamic data are consistent with the other thermodynamic data and that all the mineral thermodynamic data are consistent with reality. Reaction-path calculations at other temperatures (25 and 175°C) for these conditions and for higher and lower SiO_2(aq) activities (achieved by suppressing different precipitates) did not agree as well with observations. This limits the predicted conditions under which this group of minerals forms. The nonequilibrium restrictions (suppression of quartz and chalcedony precipitation) are very realistic for natural waters (Hem 1970). Overall, agreement between calculations and observations is quite good for this case.

The next stages of mineral evolution involve a quartz, analcime, and illite mixture followed by a quartz, albite, and potassium-feldspar mixture. The stages in this sequence have been related to zones of increasing temperature (Iijima 1978); however, reaction-path calculations done here indicate that higher temperatures alone do not change the mineral assemblage from cristobalite, zeolite, and smectite clay as long as the SiO_2(aq) activity remains high. Mineral assemblages that would result from lower SiO_2(aq) activities were determined from reaction-path calculations in which quartz was allowed to precipitate. The results show that albite is part of the mineral assemblage in that case and that analcime precipitates if albite precipitation is suppressed. Quartz, smectite clays, kaolinite, mica, and the zeolite laumontite are also part of the mineral assemblages, depending on the exact conditions (see Figs. 15 through 17). There are some areas of disagreement between calculated results and observations for this case. In particular, the aqueous-phase pH rises above the 7 to 8 range observed for Rainier Mesa water whenever the SiO_2(aq) activity is reduced to a level in equilibrium with quartz, although at 125°C the difference is small (see Fig. 4). Also, the relative potassium content tends to be low (see Fig. 6). Finally, the mineral assemblages, particularly the formation of analcime and then albite, do not occur as expected without additional constraints. Overall, the agreement between calculations and observations for this case is fair.

The reaction-path calculations discussed here can be interpreted to give an overall scheme for mineral formation at Rainier Mesa and similar NTS locations. Volcanic glass dissolution rates and slow quartz precipitation kinetics combine to give conditions necessary for precipitation of cristobalite, zeolites, and smectite clays. Because the SiO_2(aq) activity is high, zeolites such as clinoptilolite and mordenite, which have high silicon/aluminum ratios, are favored. Over longer periods of time or with increasing temperature, SiO_2(aq) activities are reduced to levels in equilibrium with quartz. Clinoptilolite and mordenite are no longer stable. Whether analcime or albite forms may depend on precipitation kinetics or may be an equilibrium process that is a function of temperature. The thermodynamic data used here indicate that kinetics must be involved if analcime precipitates, but other thermodynamic data allow equilibrium processes only. The importance of the relative dissolution rates of the volcanic glass is evident from the calculation in which congruent dissolution was assumed. The effects of glass dissolution

rates are mostly seen early in the reaction path before the mineral assemblage begins to control the aqueous-phase composition, but differences are also seen in the mineral assemblage.

Analyses of volcanic glass from Yucca Mountain are similar to the analyses of Rainier Mesa glass (Caporuscio et al. 1982; White et al. 1980). Mineral assemblages found at Yucca Mountain are also similar to those at Rainier Mesa (Caporuscio et al. 1982; Waters and Carroll 1981). Although interstitial water analyses as obtained from Rainier Mesa have not yet been made at Yucca Mountain, analyses of integral samples from a nearby well are quite similar to water found at 400 to 500 m depth at Rainier Mesa (Robinson and Beetem 1965; White et al. 1980). Because of these similarities, the models and results discussed here should be generally applicable to geochemistry at Yucca Mountain. As more data become available from Yucca Mountain, more detailed comparisons can be made.

It should be evident that these reaction-path calculations represent a very simplified model of a complex geologic system. Only the major chemical components are included in the model. It has been possible to treat glass dissolution and formation of the first-stage mineral assemblage (cristobalite, smectite clays, and zeolites) in a realistic fashion. However, limitations on current reaction-path calculation techniques have not allowed as complete an analysis of further mineral changes (where kinetics become significant) as might be desired. The calculations do represent a step in the direction of a more quantitative treatment of the relation between groundwater and mineral chemistry in tuff alteration appropriate to Yucca Mountain. In this respect, they indicate that equilibrium thermodynamics, in conjunction with some obvious rate processes, can describe much of the observed geochemistry. This is in contrast to other models for similar systems that lean more heavily on rate processes to explain observed mineralogy (Dibble and Tiller 1981).

ACKNOWLEDGEMENTS

The author thanks D. L. Bish, C. J. Duffy, A. E. Ogard, and D. T. Vaniman of the Los Alamos National Laboratory for their constructive comments on this manuscript.

REFERENCES

F. Caporuscio, D. Vaniman, D. Bish, D. Broxton, B. Arney, G. Heiken, F. Byers, R. Gooley, and E. Semarge (1982) "Petrologic studies of drill cores USW-G2 and UE25b-1H, Yucca Mountain, Nevada," Los Alamos National Laboratory report LA-9255-MS.

C. Chen (1975) "A method of estimation of standard free energies of formation of silicate minerals at 298.15 K," Am. J. Sci. 275, 801-817.

H. C. Claassen and A. F. White (1978) "Application of geochemical kinetic data to groundwater systems, a tuffaceous-rock system in Southern Nevada," in Chemical Modeling in Aqueous Systems, E. A. Jenne, Ed., Amer. Chem. Soc. Symposium Series 93, 771-793.

W. D. Dibble, Jr., and W. A. Tiller (1981) "Kinetic model of zeolite paragenesis in tuffaceous sediments," Clays Clay Miner. 29, 323-330.

E. H. Essington and J. V. Sharp (1968) "Some aspects of groundwater solution chemistry, underground nuclear explosion zones, Nevada Test Site," in Nevada Test Site, E. B. Eckel, Ed., Geol. Soc. Am. Mem. 110, 263-273.

H. C. Helgeson (1968) "Evaluation of irreversible reactions in geochemical processes involving minerals and aqueous solutions - I. Thermodynamic Relations," Geochim. Cosmochim. Acta 32, 853-877.

H. C. Helgeson, R. M. Garrels, and F. T. Mackenzie (1969) "Evaluation of irreversible reactions in geochemical processes involving minerals and aqueous solutions - II. Applications," Geochim. Cosmochim. Acta 33, 455-481.

H. C. Helgeson, T. H. Brown, A. Nigrini, and T. A. Jones (1970) "Calculation of mass transfer processes involving aqueous solutions," Geochim. Cosmochim. Acta 34, 569-592.

H. C. Helgeson, J. M. Delany, H. W. Nesbitt, and D. K. Bird (1978) "Summary and critique of the thermodynamic properties of rock-forming minerals," Am. J. Sci. 278A, 1-229.

J. D. Hem (1970) "Study and interpretation of the chemical characteristics of natural water," US Geol. Survey Water-Supply Paper 1473 (2nd ed.).

D. L. Hoover (1968) "Genesis of zeolites, Nevada Test Site," in Nevada Test Site, E. B. Eckel, Ed., Geol. Soc. Am. Mem. 110, 275-283.

A. Iijima (1978) "Geologic occurrences of zeolites in marine environments," in Natural Zeolites: Occurrence, Properties, Use, L. B. Sand and F. A. Mumpton, Eds. (Pergamon Press), pp. 175-198.

T. E. C. Keith, D. E. White, and M. H. Beeson (1978) "Hydrothermal alteration and self-sealing in Y-7 and Y-8 drill holes in northern part of Upper Geyser Basin, Yellowstone National Park, Wyoming," US Geol. Survey Professional Paper 1054-A.

J. G. Liou (1971) "Analcime equilibria," Lithos 4, 389-402.

G. K. Moncure, R. C. Surdam, and H. L. McKague (1981) "Zeolite diagenesis below Pahute Mesa, Nevada Test Site," Clays Clay Miner. 29, 385-395.

F. A. Mumpton (1977) "Natural zeolites," in Mineralogy and Geology of Natural Zeolites, F. A. Mumpton, Ed., Mineral. Soc. Am. Short Course Notes 4, 1-17.

D. C. Noble (1967) "Sodium, potassium, and ferrous iron contents of some secondarily hydrated natural silicic glasses," Am. Mineral. 52, 280-286.

J. O. Nriagu (1975) "Thermochemical approximations for clay minerals," Am. Mineral. 60, 834-839.

L. N. Plummer, B. F. Jones, and A. H. Truesdell (1976) "WATEQF - A FORTRAN IV version of WATEQ, a computer program for calculating chemical equilibria of natural waters," US Geol. Survey, Water Resources Invest. report 76-13.

R. A. Robie, B. S. Hemingway, and J. R. Fisher (1979) "Thermodynamic properties of minerals and related substances at 298.15 K and 1 bar (10^5 pascals) pressure and at higher temperatures," US Geol. Survey Bulletin 1452.

B. P. Robinson and W. A. Beetem (1965) "Chemical data on water from supply wells, Nevada Test Site," US Geol. Survey Technical Letter NTS-104.

M. L. Sykes, G. H. Heiken, and J. R. Smyth (1979) "Mineralogy and petrology of tuff units from the UE25a-1 drill site, Yucca Mountain, Nevada," Los Alamos Scientific Laboratory report LA-8139-MS.

J. R. Smyth and F. A. Caporuscio (1981) "Review of the thermal stability and exchange properties of the zeolite minerals clinoptilolite, mordenite and analcime: Applications to radioactive waste isolation in silicic tuff," Los Alamos Scientific Laboratory report LA-8841-MS.

Y. Tardy and R. M. Garrels (1974) "A method of estimating the Gibbs energies of formation of layer silicates," Geochim. Cosmochim. Acta 38, 1101-1116.

A. B. Thompson (1971) "Analcite-albite equilibria at low temperatures," Am. J. Sci. 271, 79-92.

A. C. Waters and P. R. Carroll, Eds. (1981) "Preliminary stratigraphic and petrologic characterization of core samples from USW-G1, Yucça Mountain, Nevada," Los Alamos National Laboratory report LA-8840-MS.

A. F. White (1979) "Geochemistry of ground water associated with tuffaceous rocks, Oasis Valley, Nevada," US Geol. Survey Professional Paper 712-E.

A. F. White, H. C. Claassen, and L. V. Benson (1980) "The effect of dissolution of volcanic glass on the water chemistry in a tuffaceous aquifer, Rainier Mesa, Nevada," US Geol. Survey Water-Supply Paper 1535-Q.

T. J. Wolery (1979) "Calculation of chemical equilibrium between aqueous solution and minerals: The EQ3/6 software package," Lawrence Livermore Laboratory report UCRL-52658.

T. J. Wolery (1980) "Chemical modeling of geologic disposal of nuclear waste: Progress report and a perspective," Lawrence Livermore Laboratory report UCRL-52748.

APPENDIX

This Appendix contains a list of the pure minerals and solid solutions referred to in these calculations. The formula associated with each mineral is from the EQ3/6 data base. The end members are shown for each solid solution. The three-letter combination associated with most minerals and solid solutions is the abbreviation used in the figures in this paper.

Pure Minerals

Albite (ALB) - $NaAlSi_3O_8$
Amorphous silica - SiO_2
Analcime (ANA) - $NaAlSi_2O_6 \cdot H_2O$
Calcite (CAL) - $CaCO_3$
Chalcedony - SiO_2
Cristobalite (CRI) - SiO_2
Dolomite (DOL) - $CaMg(CO_3)_2$
Gibbsite - $Al(OH)_3$
Hematite (HEM) - Fe_2O_3
Heulandite - $CaAl_2Si_7O_{18} \cdot 6H_2O$
Illite - $(Mg_{0.25}\ K_{0.6})Al_{2.3}Si_{3.5}O_{10}(OH)_2$
Kaolinite (KAO) - $Al_2Si_2O_5(OH)_4$
Laumontite - (LAU) - $CaAl_2Si_4O_{12} \cdot 4H_2O$
Muscovite (MUS) - $KAl_3Si_3O_{10}(OH)_2$
Paragonite (PAR) - $NaAl_3Si_3O_{10}(OH)_2$
Potassium-feldspar - $KAlSi_3O_8$
Prehnite - $Ca_2Al_2Si_3O_{10}(OH)_2$
Pyrophyllite - $Al_2Si_4O_{10}(OH)_2$
Quartz (QUA) - SiO_2
Talc - $Mg_3Si_4O_{10}(OH)_2$

Solid Solutions

Beidellite (BEI)

$X_{0.33}[Al_{2.33}Si_{3.67}O_{10}](OH)_2$, X = H, Na, and K

$Y_{0.165}[Al_{2.33}Si_{3.67}O_{10}](OH)_2$, Y = Ca and Mg

Clinoptilolite (CLI)

$X_2[Al_2Si_{10}O_{24}]\cdot 8H_2O$, X = Na and K

$Y[Al_2Si_{10}O_{24}]\cdot 8H_2O$, Y = Ca and Mg

Mordenite (MOR)

$X[AlSi_5O_{12}]\cdot 3H_2O$, X = Na and K

Nontronite (NON)

$X_{0.33}[Al_{0.33}Si_{3.67}Fe_2O_{10}](OH)_2$, X = H, Na, and K

$Y_{0.165}[Al_{0.33}Si_{3.67}Fe_2O_{10}](OH)_2$, Y = Ca and Mg

Plagioclase (PLA)

Low albite - $NaAlSi_3O_8$

Anorthite - $CaAl_2Si_2O_8$

Saponite (SAP)

$X_{0.33}[Al_{0.33}Si_{3.67}Mg_3O_{10}](OH)_2$, X = H, Na, and K

$Y_{0.165}[Al_{0.33}Si_{3.67}Mg_3O_{10}](OH)_2$, Y = Ca and Mg

Sodic muscovite (SOD)

Paragonite - $NaAl_3Si_3O_{10}(OH)_2$

Muscovite - $KAl_3Si_3O_{10}(OH)_2$

☆U.S. GOVERNMENT PRINTING OFFICE: 1983-0-776-026/120

Printed in the United States of America
Available from
National Technical Information Service
US Department of Commerce
5285 Port Royal Road
Springfield, VA 22161

Microfiche (A01)

Page Range	NTIS Price Code	Page Range	NTIS Price Code	Page Range	NTIS Price Code	Page Range	NTIS Price Code
001-025	A02	151-175	A08	301-325	A14	451-475	A20
026-050	A03	176-200	A09	326-350	A15	476-500	A21
051-075	A04	201-225	A10	351-375	A16	501-525	A22
076-100	A05	226-250	A11	376-400	A17	526-550	A23
101-125	A06	251-275	A12	401-425	A18	551-575	A24
126-150	A07	276-300	A13	426-450	A19	576-600	A25
						601-up*	A99

*Contact NTIS for a price quote.

Los Alamos